Eksplorium
Volume 45 No. 1, May 2024: 1–16

p-ISSN 0854-1418
e-ISSN 2503-426X

Distribution and Characteristics of Rare Earth Elements in Uranium-Ore Deposits from Rirang Area, West Kalimantan Province, Indonesia

Tyto Baskara Adimedha[1*], Rayhan Aldizan Farrenzo[2], I Gde Sukadana[1], Rosmalia Dita Nugraheni[2], Fadiah Pratiwi[1], Roni Cahya Ciputra[1], Frederikus Dian Indrastomo[1], Heri Syaeful[1], Yoshi Rachael[1]

[1]Research Center for Nuclear Material and Radioactive Waste Technology, ORTN-BRIN
KST B. J. Habibie, South Tangerang, Banten, 15314, Indonesia
[2]Department of Geological Engineering, Faculty of Earth Technology and Energy, Universitas Trisakti
Letjen S. Parman St., No.1, Campus A, West Jakarta, DKI Jakarta, 11440, Indonesia
*E-mail: tyto001@brin.go.id

Article received: 15 May 2024, revised: 30 May 2024, accepted: 31 May 2024
DOI: 10.55981/eksplorium.2024.7058

ABSTRACT

Uranium and rare earth elements (REE) are essential elements for the development of green environmentally friendly, and sustainable energy. To meet the increasing demand for these raw materials, Indonesia has taken steps to explore and map potential deposits, including the Rirang Sector in Melawi Regency, West Kalimantan. However, the available information on the mineralization of these elements in the area is limited. Therefore, this study aimed to provide a detailed characterization on the petrology and geochemical characteristics of uranium ore and to synthesize the mineral genesis of uranium and REE-bearing ore in the Rirang Sector. The analytical methods used included petrography, micro-XRF, and geochemical analysis. The results showed that uranium mineralization was present in brannerites, uranophane, and swamboite associated with tourmaline and monazite ore. Similarly, REE concentrations were hosted by REE-bearing minerals, such as monazite, xenotime, and loparite. Geochemically, the uranium concentration in the monazite ore ranged from 1,110–28,440 ppm, while the total REE (TREE) concentration varied between 85,320 to 138,488 ppm. The formation of uranium and REE mineralization were due to the metasomatism process and its association with the Na-rich fluid of felsic intrusion. Notably, the weathering process did not enrich uranium and REE content in the soil but rather decreased it due to the leaching process and the absence of clay minerals capable of absorbing the REE cations on the surface of clay crystal structures.

Keywords: West Kalimantan, monazite, rare earth elements, tourmaline, uranium

INTRODUCTION

Developing clean and efficient technologies is imperative to reduce carbon emissions and combat global warming, specifically as technology continues to advance rapidly. While renewable energy sources such as solar, hydro, and wind power are being prioritized in Indonesia, nuclear energy presents as a viable option for generating green energy. Developing those energy sources requires critical materials such as uranium for the nuclear fuel and rare earth elements (REE) for the MiMH battery component.

The exploration of uranium and REE is necessary to prepare the raw component for developing green and clean energy. One promising prospect of uranium and REE in Indonesia is located in Kalan Area, Melawi Regency, West Kalimantan [1], [2]. Some sectors in the Kalan area with uranium and REE potential are Tanah Merah, Jeronang, Indramayu, Jumbang, Dendang Arai, and Rirang [2]. In the Rirang Sector, uranium and

REE-bearing ore consist of monazite and tourmaline ore. The average total rare earth oxides (REO) in monazite ore is 62,74%, and in tourmaline, the REO is 3.62% [2]. Uranium and REE resources in the Rirang area are estimated at approximately 227 tonnes of uranium and 3,917.59 tonnes of REO [2].

Mineralization signatures in the Rirang area consist of uraninite, monazite, tourmaline, pyrite, ilmenite, ilmenorutile, xenotime, and apatite [1], [3]–[5]. However, there is no other study on the distribution of the ore mineralization for the coeval REE and uranium. Therefore, this study aims to characterize the ore's petrology and geochemical characteristics and synthesize the mineral genesis of uranium and REE-bearing ore in the Rirang Sector, West Kalimantan.

REGIONAL GEOLOGY

The Kalan area is occupied by predominant metamorphic, metasedimentary, intrusive, and volcanic rocks. Metamorphic rocks include quartzite, hornfels, and mica schist. These rocks are composed of quartz, biotite, and muscovite with accessory minerals such as tourmaline, andalusite, corundum, stilpnomelane, pyrophyllite, molybdenite, epidote, and sericite. The metasedimentary rocks consist of Jeronang metasiltstone, metasiltstone, meta-argillite, Jeronang metapelite, tuffaceous metapelite, and interbedding metasiltstone and metapelite. The metasiltstone-metapelite interbedding mainly hosts uranium ore in the Kalan area (Figure) [1], [2], [4]–[6].

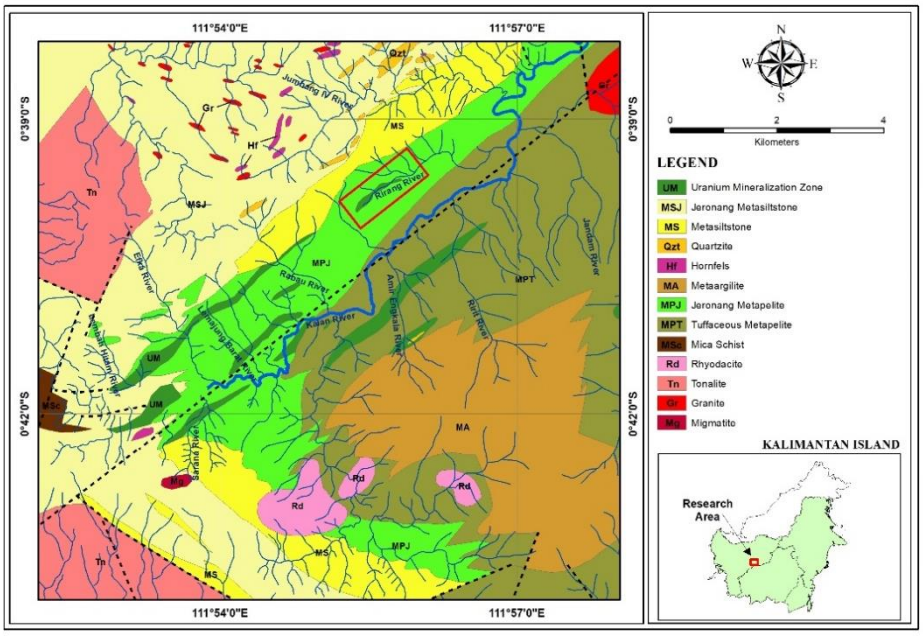

Figure 1. Geological Map of the Kalan Area, West Kalimantan. The Rirang Sector consists of the Jeronang Metapelite and Uranium Mineralization Zone (modified from [1], [2])

The metamorphic and metasedimentary rocks in the Kalan area were intruded by Sukadana Granite, Sepauk Tonalite, and Rhyodacite volcanic rocks. Both Sukadana Granite and Sepauk Tonalites are classified as Cretaceous intrusive rocks. Meanwhile, Rhyodacite volcanic is classified as Oligocene to Miocene Sintang Intrusive rock.

p-ISSN 0854-1418
e-ISSN 2503-426X

Sukadana Granite is composed of quartz, orthoclase, plagioclase, biotite, zircon, and epidote. Sepauk Tonalite is primarily composed of biotite, hornblende, and plagioclase. Rhyodacite volcanic rock in the area consists of biotite, hornblende, oligoclase, andesine, and quartz, with some being shallow intrusions of sill or dike [1], [2].

The Rirang Sector consists of frequently weathered metasiltstone and metapelite. The bedding orientation is NNE-SSW and dipping 77°–86° directing to WNW [3], [4]. The foliation structure is ENE-WSW oriented with a dip of 40°–84° to NNW [3]. Subsequently, metasiltstone is generally composed of quartz and feldspar, with a minor amount of biotite and muscovite. The alteration minerals found in metasiltstone are chlorite, sericite, tourmaline, pyrite, and hematite. The metapelite exhibits a spotted shale texture with a unidirectional foliation structure. The spotted shale texture is interpreted as andalusite altered to fine sericite, muscovite, and quartz minerals. The metasiltstone and metapelite rocks are classified as greenschist facies [5].

The ore mineralization in the Rirang Sector is mainly found in boulder size and classified into two groups, tourmaline ore boulder and monazite ore boulder. Uranium and REE-bearing minerals consist of uraninite, brannerite, monazite, and xenotime. These minerals are associated with other ore minerals such as molybdenite, ilmenorutile, ilmenite, tourmaline, and apatite [5].

METHODOLOGY

Samples were collected from the field along the Rirang River and represented by barren host rock, monazite ore, tourmaline ore, and weathered soil derived from monazite ore (Table 1). A total of 16 samples consisting of 2 barren host rocks, 7 monazite ores, 1 tourmaline ore, and 6 weathered soils were analyzed. This investigation's analytical methods included petrography, micro-XRF, and geochemical analysis. Petrography analysis was conducted using Leitz Laborlux 11 Pol and Nikon Eclipse E200 Polarization Microscope at Trisakti University, Indonesia. A total of 8 were analyzed petrographically to define the mineral composition, texture, and characteristics.

Table 1. Sample types and analyses

No.	Sample Code	Sample Type	Analyses		
			Petrography	Micro-XRF	XRF and ICP-MS
1	RR02.3	Host Rock	x	x	
2	RR09	Host Rock	x	x	x
3	RR02	Tourmaline Ore	x	x	
4	RR04	Monazite Ore	x	x	
5	RR07	Monazite Ore	x	x	x
6	RR10	Monazite Ore	x	x	
7	RR13	Monazite Ore			x
8	RR17	Monazite Ore	x	x	
9	RR18	Monazite Ore			x
10	RR23	Monazite Ore	x	x	
11	RHS03	Soil			x
12	RHS05	Soil			x
13	RHS07	Soil			x
14	RHS09	Soil			x
15	RHS11	Soil			x
16	RHS15	Soil			x

Micro-XRF analysis was used to identify the elemental distribution in ore and host rock. This analysis was conducted using Bruker M4 Tornado Plus available in The Research Centre for Nuclear Fuel Cycle and Radioactive Waste Technology, The National Research and Innovation Agency, Indonesia. A total of 8 ore and host rock samples were prepared in the form of a 5 x 5 cm smooth surface slab sample. During data acquisition, a pixel size of 35 µm was used to analyze a total area of approximately 30 x 30 mm. The X-ray tube was operated at 50kV and 600 µA, and a pixel time of 12 ms/pixel. The resulting maps were processed using Bruker M4 Tornado software to extract the elemental map from the sample. The analysis was continued using Advanced Mineral Identification and Characterization System (AMICS) software to determine the mineralogical composition of the sample [7], [8].

The geochemical analysis involved applying X-ray Fluorescence (XRF) and Induced Couple Plasma-Mass Spectrometry (ICP-MS). The XRF was used to determine major oxide composition and ICP-MS to identify trace elements in the samples. A total of 10 samples were analyzed at Indomineral Research, Indonesia, using Bruker S8 Tiger II for XRF analysis and Agilent 7900 ICP-MS for ICP-MS analysis. In this study, both Micro-XRF and XRF were used, with the former providing an advantage in elemental mapping across the samples, while the latter offered higher accuracy in quantification. Therefore, the use of dual analyses, remains relevant in this investigation.

RESULTS

Mineralogy

The host rock sample RR02.3 is a metapelite showing phyletic foliation with epiblastic-hypidioblastic texture. Foliation structures are evidenced by the linear alignment of fine clays composed of illite, kaolinite, chlorite, and wonesite. The AMICS analysis confirms the linear orientation of illite, kaolinite, and chlorite, and also identified other mineral compositions, such as almandine, cordierite, andalusite, staurolite, and tourmaline (Figure 2), that are usually present in trace amounts. Host rock sample RR09 is identified as metasiltstone, with slaty cleavage with lepidoblastic and xenoblastic texture. The mineralogy of the sample is composed of muscovite, oligoclase, and illite. Muscovite alters to a clay mineral with weathering, and hematite is found as a vein. The AMICS analysis indicates that the clay minerals in the metasilt are montmorillonite, illite, chlorite, and kaolinite. Metasiltstone also contains beryl and tourmaline in very small amounts.

Tourmaline ore, represented by RR02, shows a tourmaline vein with a predominant mineral composition of wonesite and polycrystalline quartz (Figure 3). Apatite occupies the edge of the tourmaline vein, and monazite is identified as an accessory mineral in the sample. The ore minerals found in the sample are rutile, magnetite, ilmenite, and brannerite. Brannerite and monazite are identified as uranium and REE-bearing minerals in the tourmaline ore. The AMICS analysis shows that erlianite and apatite are formed and occupy the edge of the vein. Brannerite and uranophane are found in uranium-bearing veins and are associated with xenotime, monazite, and apatite.

p-ISSN 0854-1418
e-ISSN 2503-426X

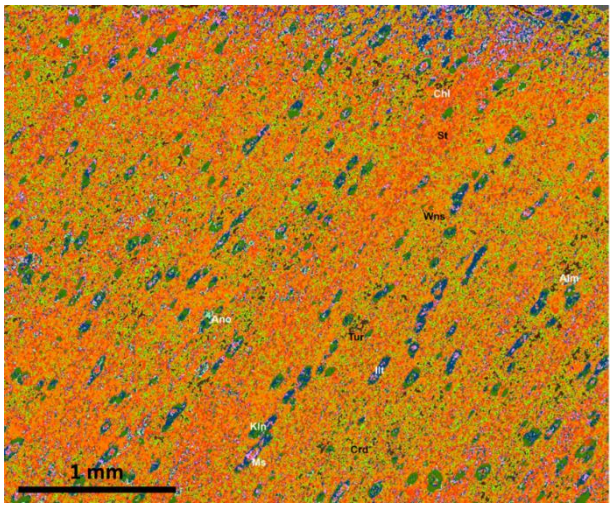

Figure 2. The AMICS results of metapelite host rock show spotted shale texture representing the foliation orientation. (Alm= almandine, Ano= anorthite, Chl= chlorite, Crd= cordierite, Ilt=illite, Kln=kaolinite, Ms=muscovite, St=staurolite, Wns=wonesite. The AMICS results of metapelite host rock show spotted shale texture representing the foliation orientation. (Alm= almandine, Ano= anorthite, Chl= chlorite, Crd= cordierite, Ilt=illite, Kln=kaolinite, Ms=muscovite, St=staurolite, Wns=wonesite. Mineral abbreviation after [9]

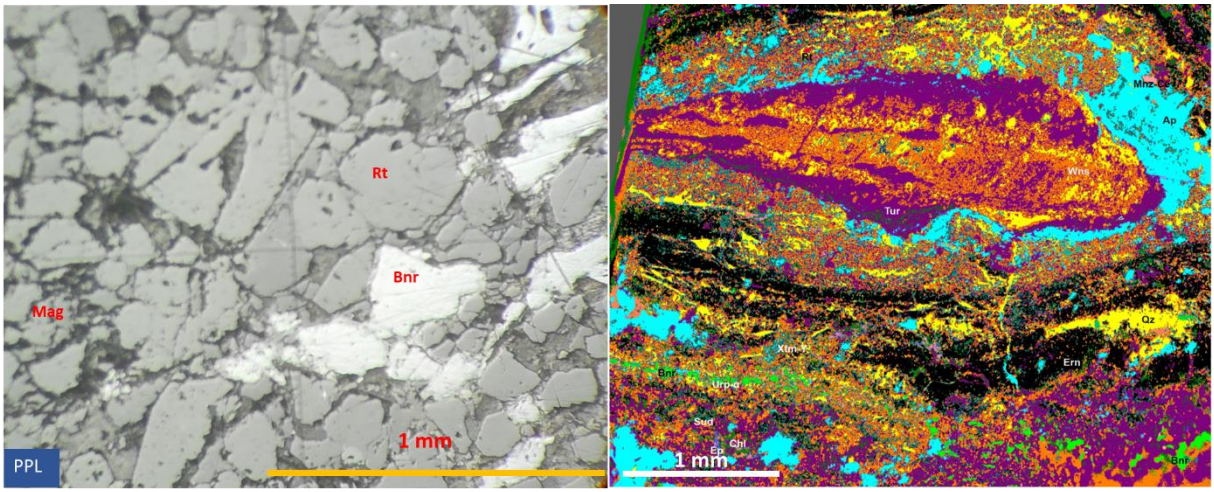

Figure 3. Microphotograph and AMICS result of tourmaline ore. Ore microphotograph shows brannerite as a uranium-bearing mineral associated with magnetite and rutile. AMICS result shows tourmaline vein associated with apatite, brannerite, and uranophane that cut the tourmaline ore (Ap= apatite, Bnr= brannerite, Chl= chlorite, Ep=epidote, Ern=erlianite, Mag = magnetite, Mnz-Ce=monazite-Ce. Qz=quartz, Rt=rutile, Sud=sudoite, Tur=tourmaline, Urp-α= uranophane, Xtm-Y= xenotime-Y. Mineral abbreviation after [9]

The monazite ore is dominated by an ore body of monazite with a uranium-bearing vein that cross-cuts the ore body. Monazite occurs in the form of polycrystalline grain having irregular and sutured boundaries. Accessory minerals found in the monazite ore include apatite, xenotime, tourmaline, ilmenite, rutile, pyrite, molybdenite, magnetite, quartz, hornblende, chlorite, and hematite. The quartz crystals are found in between monazite crystals. Almandine, cordierite, sudoite, and copper mineral are identified using AMICS analysis.

Uranium-bearing minerals found in the monazite ore are identified as brannerite and uranophane. These minerals are found in veins or spotted minerals associated with molybdenite, magnetite, rutile, ilmenite, and hematite. In addition, brannerite is found in prismatic form or irregular aggregates,

despite a few brannerites occurring as deformed minerals (Figure 4). Molybdenites appear as irregular deformed-shaped inclusion of monazite. Based on AMICS analysis, swamboite presents as a secondary uranium-bearing mineral in the monazite ore.

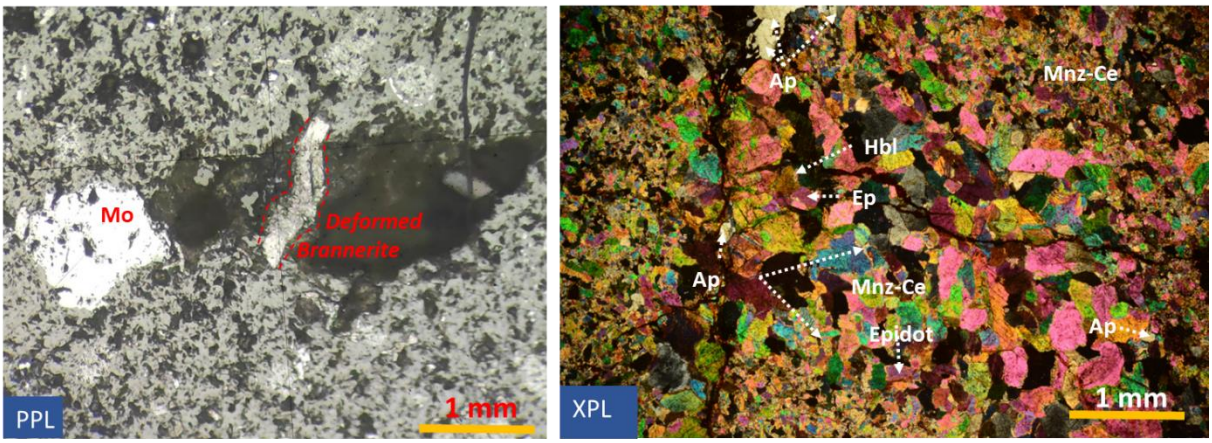

Figure 4. Microphotograph of monazite ore showing deformed brannerite, molybdenite, and polycrystalline monazite associated with apatite and epidote (Ap= apatite, Hbl= hornblende, Ep= epidote, Mnz-Ce = monazite, Rt= rutile, Mo= molybdenite. Mineral abbreviation after [9]

Elemental Distribution

The elemental distribution of host rock samples (RR.02.3 and RR09) is predominated by Si, Al, Fe, and K (Figure 5). These elements usually occur in silicate minerals such as K-feldspar, mica, and clays. These elements form a clay mineral that dominates the host rock sample in the form of wonesite, illite, kaolinite, montmorillonite, and chlorite. Other minerals composed of these elements are muscovite, oligoclase, albite, biotite, staurolite, and cordierite.

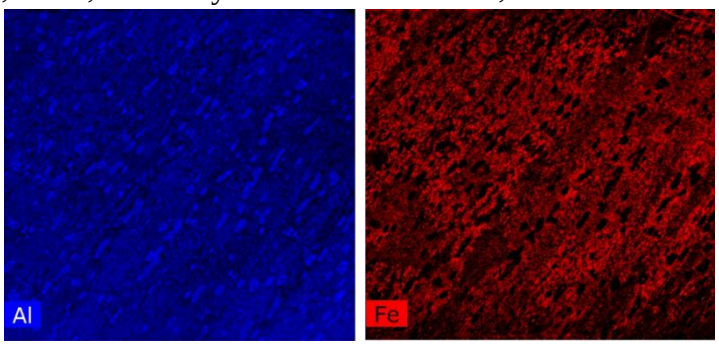

Figure 5. The distribution of dominant elements such as Al and Fe in the host rock sample indicates K-feldspar, mica, and clays distribution

Uranium and REE are mainly found in the tourmaline and monazite ore samples. Si, Al, Fe, and Mg dominate the major element of tourmaline ore. These elements are found in tourmaline and wonesite minerals that are dominant in the sample. Uranium distribution in tourmaline ore concentrated along the veinlet associated with the Y element. The REE distribution can be divided into two groups, the Ce-Nd and Y groups. The Ce-Nd elements are closely associated and distributed randomly in the sample. On the other hand, Y is concentrated along the veinlet and at the edge of the tourmaline ore (Figure 6). The U-Y assemblages are incorporated in brannerite minerals, whereas Ce-Nd elements are incorporated in monazite, and Y s found in xenotime.

p-ISSN 0854-1418
e-ISSN 2503-426X

The elemental distributions in sample RR10, as monazite ore samples (Figure 7), are composed of Ce, La, P, and Nd, representing the monazite mineral. Uranium is distributed along the crack of the sample in the form of brannerite, uranophane, and swamboite minerals. The cracks are filled with elements such as Fe, Si, Cu, and Mo. The Fe is incorporated either in almandine or chlorite; Si represents quartz, Cu represents the occurrence of native copper, and Mo represents molybdenite. REE in the monazite ore sample includes Ce, La, Nd, Sm, Gd, and Y. The last element is the primary element found in xenotime. Furthermore, Gd occurs in trace amount and mainly form loparite mineral, and uranium distribution in monazite ore is associated with the Y element in several veins or cracks. But the other REE elements, such as Ce, La, Nd, Sm, and Gd are the dominant element across the samples, indicating that the monazite ore is formed before the uranium mineralization.

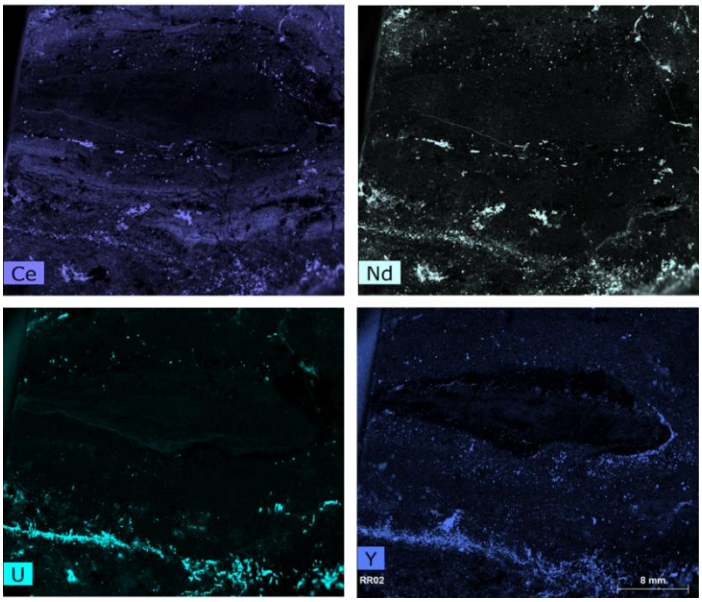

Figure 6. Distribution of uranium and REE in a tourmaline ore sample

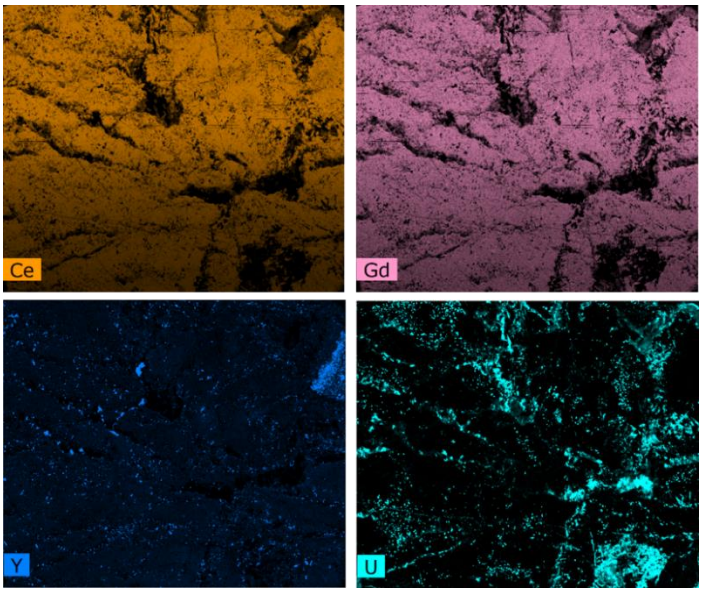

Figure 7. Distribution of uranium and REE in a monazite ore sample

Geochemistry

SiO_2 appears as the major element in the soil and host rock samples (ranges from 46.23 to 64.74%), much higher than the constituent in the monazite ore (1.46–16.73%). Subsequent major oxide compositions are Fe_2O_3, Al_2O_3, and K_2O (Table 2). The silicate minerals dominate the soil and host rock and have undergone a weathering process, forming clays. In contrast, major oxides, such as CaO, MgO, MnO, Cr_2O_3, and P_2O_5, are relatively higher in monazite ore than in the soil or host rock sample. The presence of ore minerals such as monazite, apatite, and tourmaline cause the high concentration of these elements in monazite ore.

Table 2. Mayor oxide composition (wt.%) of soil, host rock, and monazite ore from the Rirang Sector

Element	Soil						Host Rock	Monazite Ore		
	RHS03	RHS05	RHS07	RHS09	RHS11	RHS15	RR09	RR07	RR13	RR18
SiO_2	49.29	60.21	64.74	49.77	46.23	50.06	61.93	7.67	16.73	1.46
Fe_2O_3	9.31	7.10	12.17	8.27	13.65	12.81	7.14	2.19	3.03	1.13
Al_2O_3	27.76	21.68	15.42	29.62	27.23	25.27	20.45	5.83	12.98	1.31
CaO	<0.01	<0.01	<0.01	<0.01	<0.01	<0.01	0.56	3.77	0.29	0.06
MgO	0.25	0.25	0.17	0.43	0.28	0.17	1.28	0.52	1.18	0.78
MnO	<0.01	<0.01	0.01	0.01	0.01	0.01	0.06	0.20	0.16	0.25
Cr_2O_3	0.01	0.03	0.05	0.14	0.02	0.01	0.02	1.35	1.30	1.68
Na_2O	1.28	1.05	0.74	2.25	1.07	1.31	1.74	1.90	1.63	1.38
K_2O	4.39	1.75	0.51	6.09	2.67	3.44	2.65	2.71	2.55	0.53
TiO_2	1.22	1.03	0.95	1.36	1.22	1.34	0.90	0.48	1.50	1.16
P_2O_5	0.13	0.12	0.30	0.05	0.08	0.09	0.29	16.11	10.72	17.49
LOI %	8.42	8.38	7.21	7.35	10.31	7.67	4.45	2.55	3.32	0.87

The highest uranium concentration is found in monazite ore sample RR07, reaching 28,440 ppm, followed by other monazite ore RR18 (3,230 ppm), and RR13 (1,110 ppm). In the host rock sample, the uranium concentration reaches 391.96 ppm. In the soil sample, the uranium concentrations vary between 38.72–241.76 ppm (Table 3), indicating that the uranium element has leached out during weathering and is concentrated mainly in the ore body of monazite and tourmaline ores. The total REE (TREE) concentration in monazite ore is about 85,320–13,8488 ppm. REE in monazite ore is dominantly composed of light REE (LREE), with concentrations ranging from 81,813 to 133,772 ppm. Meanwhile, heavy REE (HREE) concentration ranges from 1,472 to 2,532 ppm (Table 4).

The variation diagram of uranium compared to several major oxides and trace elements (Figure 8) shows that uranium has a positive correlation with Na_2O and P_2O_5, indicating that uranium-bearing minerals are chemically composed of elements such as brannerite, uranophane, swamboite, loparite, and monazite. The positive correlation between uranium and P_2O_5 also indicates that apatite and xenotime form co-genetically during uranium mineralization [10]. On the contrary, the negative correlation between uranium and Al_2O_3 and Fe_2O_3 indicates that uranium is not associated with silicate and ferrous minerals such as clays and ferromagnesian minerals.

Compared to other elements, uranium exhibits a relatively strong positive correlation with marker elements of hydrothermal alteration products, including Cu, Mo, V, and Pb. Positive correlation suggests that these elements are enriched during the uranium mineralization process. U-Cu and U-Mo correlation shows relatively higher enrichment in the soil sample than

other elements. Mo and Cu are believed to be adsorbed to the clay mineral during the weathering process. They are derived from the leaching process of host minerals, such as biotite, magnetite, hornblende K-feldspar, plagioclase, and ilmenite [11].

Table 3. Trace elements composition (ppm) of soil, host rock, and monazite ore from the Rirang Sector

Element	Soil					Host Rock		Monazite Ore		
	RHS03	RHS05	RHS07	RHS09	RHS11	RHS15	RR09	RR07	RR13	RR18
Li	15.9	12.0	5.0	16.0	18.7	17.9	47.5	3.4	15.8	2.9
Be	1.9	1.1	1.0	2.0	2.1	2.4	2.6	0.5	1.2	0.4
V	184.6	164.2	240.9	187.1	218.7	190.5	134.3	312.8	199.5	82.3
Co	8.4	8.7	9.2	6.0	8.7	8.9	37.6	2.6	4.8	1.2
Ni	74.0	59.2	154.8	48.8	90.4	126.0	75.1	1.5	6.5	<0.001
Cu	40.5	34.5	78.5	29.3	35.2	48.5	34.8	3.4	112.1	24.9
Zn	11.2	9.6	15.8	12.1	10.3	4.2	56.9	5.2	4.5	0.2
Ga	38.1	30.9	35.0	36.2	35.2	38.9	58.6	879.7	1,087.7	1,582.4
As	16.5	19.8	15.0	14.3	20.8	15.0	27.1	189.7	312.8	516.9
Se	3.0	1.7	5.5	0.5	1.0	1.4	14.0	243.1	322.3	456.1
Rb	209.7	86.1	23.5	248.9	177.3	232.6	169.1	9.9	82.0	1.3
Sr	21.3	19.2	35.3	13.0	33.3	32.4	105.6	50.8	142.4	26.3
Zr	88.0	71.5	50.8	77.1	70.8	85.3	57.3	2.8	160.3	38.2
Nb	10.7	5.5	11.7	15.5	5.5	4.0	5.5	24.2	66.7	60.4
Mo	2,540.0	149.3	44.1	135.1	209.9	18.4	95.6	4,740.0	283.7	592.8
Ag	0.1	0.1	0.1	0.2	0.1	0.2	0.1	0.2	0.3	0.1
Cd	4.6	0.5	0.3	0.5	0.6	0.3	0.4	1.0	0.9	1.0
Sn	1.7	3.0	4.1	1.6	0.9	0.4	6.6	2.0	1.7	<0.001
Sb	0.2	0.3	0.4	0.2	0.5	0.3	0.5	0.7	0.4	0.1
Te	0.2	0.2	0.2	0.1	0.1	0.1	0.1	0.4	0.4	0.2
Cs	3.8	2.8	1.4	3.9	5.7	6.4	6.5	0.5	0.9	0.2
Ba	481.8	250.2	77.2	568.4	281.1	372.6	316.6	53.2	575.4	17.9
Hf	2.5	2.2	1.9	2.4	1.9	2.5	2.0	11.8	14.4	18.4
Ta	0.9	0.7	1.1	1.3	0.5	0.5	0.7	2.1	2.9	3.0
W	4.7	3.4	6.5	5.5	2.1	1.3	3.4	19.7	39.0	13.8
Pb	59.7	25.2	115.2	27.6	6.7	6.9	88.2	3,840	1,260	1,550
Bi	0.3	0.4	0.5	0.2	0.2	0.2	0.4	0.4	0.6	0.2
Th	22.2	42.3	33.3	20.8	20.0	27.6	17.1	20.3	24.6	36.9
U	184.2	38.7	241.8	107.5	84.4	91.4	392.0	28,440.0	1,110.0	3,230.0

Table 4. REE composition (ppm) of soil, host rock, and monazite ore from the Rirang Sector

Element	Soil					Host Rock		Monazite Ore		
	RHS03	RHS05	RHS07	RHS09	RHS11	RHS15	RR09	RR07	RR13	RR18
La	192.1	119.3	381.8	30.2	44.3	102.9	840.2	18,420	24,710	34,960
Ce	401	254.5	593.4	65.8	69.5	131.7	1,630	39,220	46,400	> 50000
Pr	45.5	27.1	89.3	6.1	9.9	20.6	194.9	4,560	5,130	8,730
Nd	156.3	84.9	286.7	18.8	28.8	54.8	651.1	15,170	16,290	31,360
Sm	27.5	13.7	46.8	3.5	4.8	8.1	127.6	2,960	3,080	5,860
Eu	2.8	1.4	4.2	1	0.9	1.1	6.5	123.6	134.9	182
Gd	12.8	6.8	19.7	1.8	2.1	3.6	55.9	1,360.00	1,520.00	2,680.00
Tb	1.6	0.8	2.5	0.2	0.3	0.4	7.4	180.7	182.9	324.2
Dy	9.1	4.3	16.6	1.6	2.1	2.6	41.4	1,090.00	952.4	1,620.00
Ho	1.1	0.6	2.2	0.2	0.3	0.3	4.8	136.6	104.1	176.4
Er	2	1.1	3.9	0.6	0.7	0.8	8.3	239.4	149.4	257.9
Tm	0.3	0.1	0.4	0.1	0.1	0.1	0.9	27.4	13.9	24.8
Yb	1.6	1	2.3	0.7	0.9	0.9	4.8	140.9	57.3	106.3
Lu	0.2	0.1	0.3	0.1	0.1	0.1	0.7	19.7	12.1	22.8
Sc	28.4	23.8	30.3	35	36.4	32.6	22.3	32.4	20.5	4.7
Y	10.4	8.5	22.9	3.6	4.8	4.9	76.4	1,640.00	1,130.00	2,180.00
TREE	892.8	548.2	1,503.30	169.2	206	365.5	3,673.30	85,320.80	99,887.40	138,488.90
$(La/Yb)_N$	79	84.1	113.7	30.3	34.9	80.3	118.7	88.3	291.3	222.3
$(La/Sm)_N$	4.4	5.5	5.1	5.4	5.8	8	4.1	3.9	5	3.8
$(Gd/Yb)_N$	6.3	5.8	7	2.2	2	3.4	9.5	7.8	21.5	20.4

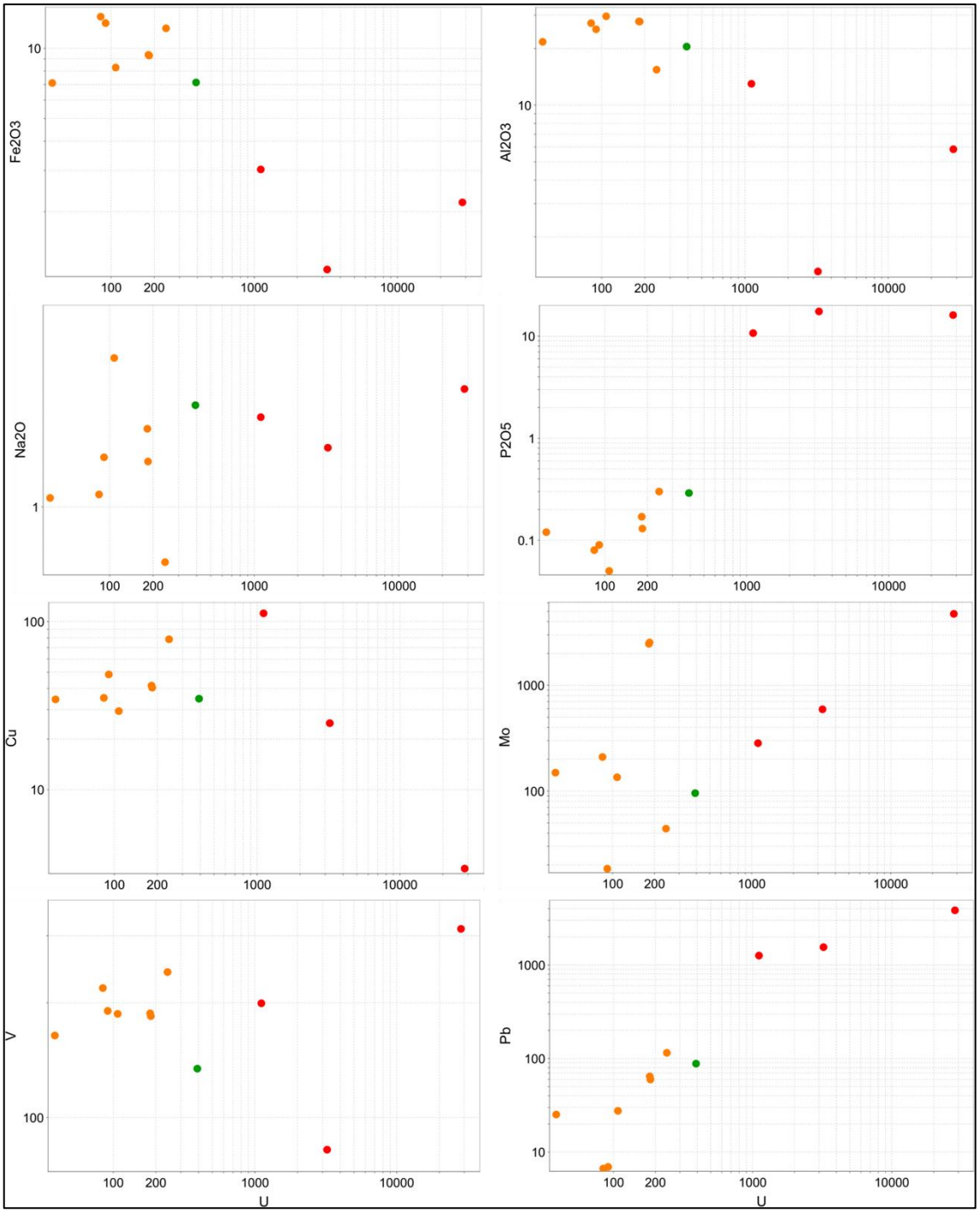

Figure 8. Variation diagram of uranium versus several major oxides and trace element.

The variation diagram of TREE and several major oxides, uranium, and trace element (Figure 9) shows positive correlations with Na_2O and P_2O_5, indicating that REE are mainly incorporated into phosphate or sodium oxide minerals as the REE-bearing minerals such as monazite, xenotime, apatite, and loparite. Mn oxide plays an important role in the distribution of REE because Mn oxides can bind REE through several processes, such as coprecipitation, adsorption, and ion exchange [12]. The Na_2O and REE tend to become enriched in post-magmatic hydrothermal

p-ISSN 0854-1418
e-ISSN 2503-426X

fluids. As a result, these elements are often closely associated with each other. On the other hand, TREE shows a negative correlation to Al_2O_3 and Fe_2O_3, indicating that REE is not enriched in clay-rich rocks or highly weathered soil. TREE shows a positive correlation compared to uranium and other trace elements such as Cu, V, and Pb. The data indicate that TREE and uranium are co-genetically concentrated during hydrothermal alteration.

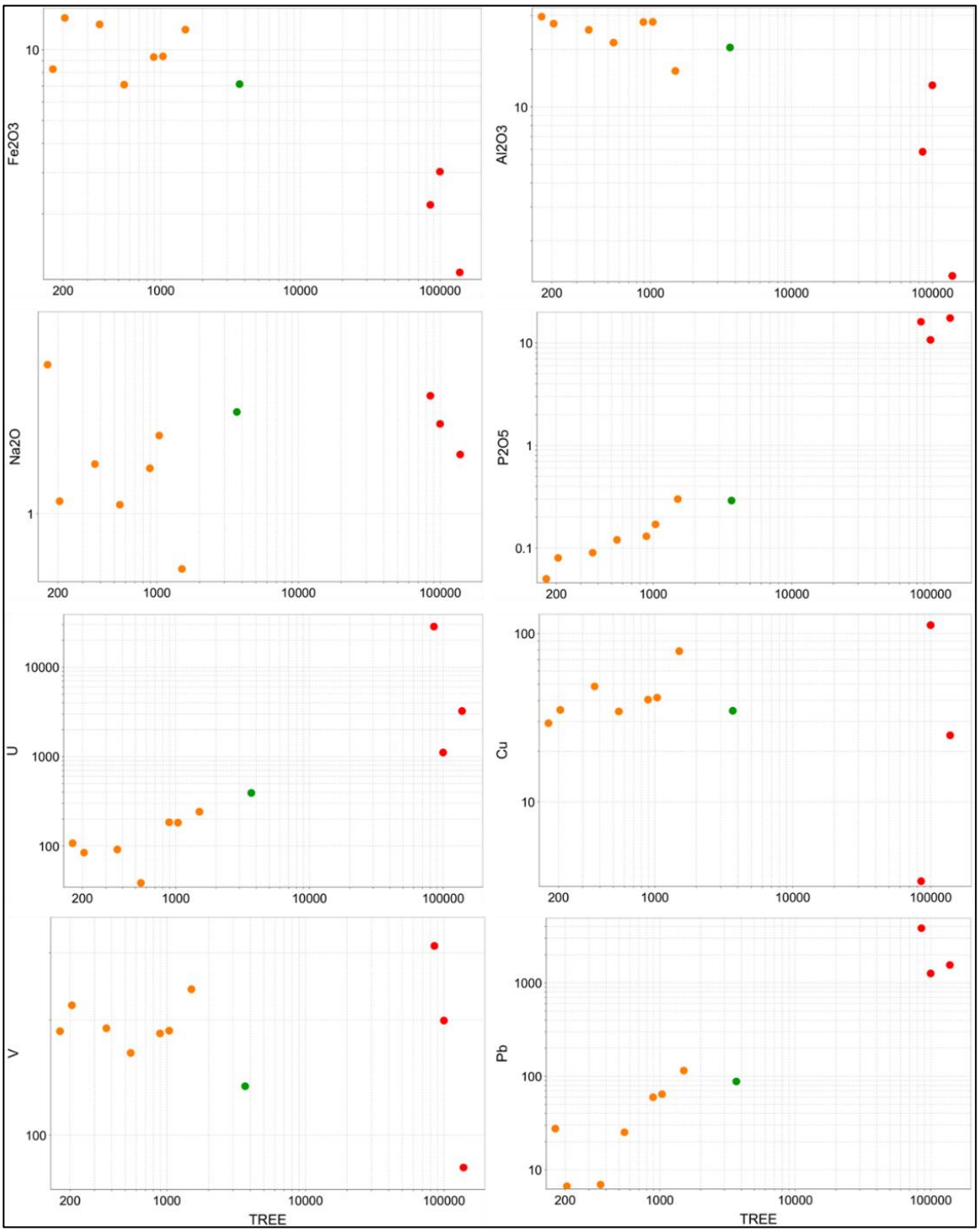

Figure 9. Variation diagram of TREE versus several major oxides and trace elements

The C1 Chondrite normalization [13] in the trace element diagram (Figure 10a) shows that the HFSE and LILE exhibited a greater depletion pattern than the Upper Continental Crust (UCC) [14] and the Post Archean Australian Shale (PAAS) [15]. On the other hand, uranium and REE show enrichment patterns, except for Eu, which shows depletion. The Eu depletion, followed by Sr and K depletion, indicates the weathering process of plagioclase [16]. In addition, the Eu depletion also indicates plagioclase fractionation in the magma source [12], [14].

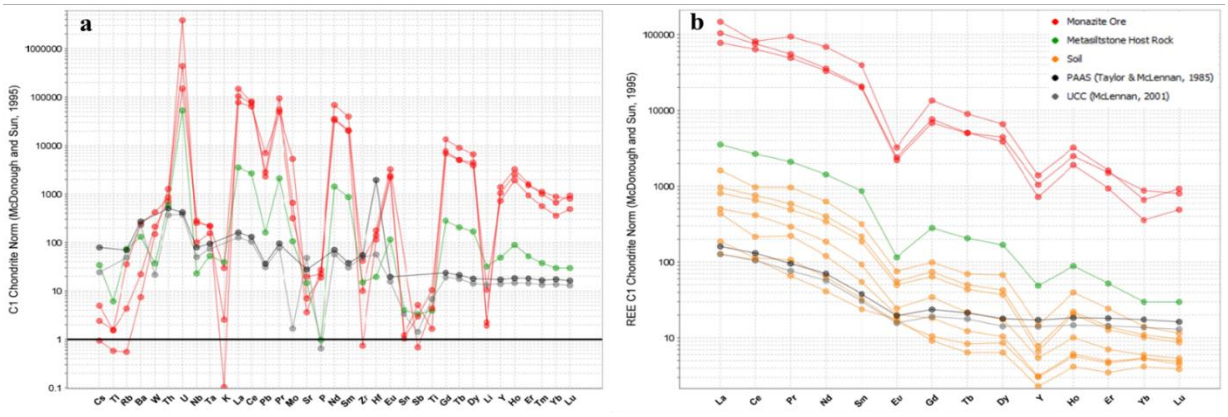

Figure 10. The multi-element plot of monazite ore, host rock, and soil in the Rirang Sector, West Kalimantan. a) Monazite ore and metasiltstone host rock show a depletion pattern in HSFE and LILE and enrichment in uranium and REE. b) Monazite ore, host rock, and soil show enrichment patterns in LREE and depletion patterns in HREE

The multi-element diagram of the REE-C1 chondrite (Figure 10b) shows an LREE enrichment and an HREE depletion pattern. These patterns indicate two alteration types during the uranium mineralization process, K-feldspar alteration and silicification [17], [18]. These patterns are also similar to the typical monazite that probably act as the main source of REE analyzed in the sample. The REE pattern in the soil sample shows similarity to the ore and host rock sample but has a lower value. The lower value indicates an early leaching phase of weathering process [19], [20].

DISCUSSIONS

The host rock for uranium and REE mineralization in the Rirang Sector are metamorphic rocks, including metapelite and metasiltstone. The metamorphic rocks were characterized by slaty to phyllitic foliation and spotted shale textures. The spotted shale texture is a result of clay minerals from weathered andalusite minerals, like wonesite and kaolinite. The occurrences of almandine, cordierite, and staurolite minerals indicate the regional metamorphism process. Paragenesis consisting of muscovite, almandine, and andalusite minerals indicates that the area's metamorphism facies were greenschist facies.

The rocks' REE pattern and Eu anomaly indicate the source rock characteristics [15]. A high LREE/HREE ratio and negative Eu anomaly are commonly found in granitic rocks [21]–[23]. The C1 Chondrite normalized REE plot shows a fractionated REE pattern ((La/Yb)N = 88.31–291.34, mean = 180.15), characterized by highly fractionated LREE ((La/Sm)N = 3.75–5.05, mean = 4.21) and HREE ((Gd/Yb)N = 7.82–21.49, mean = 14,8). In addition, REE pattern shows negative Eu anomaly, positive Ce

anomaly, and enriched LREE/HREE ratio. This suggests that meta-siltstone and monazite ore are derived from felsic source rocks [24]. The granite intrusions north of the Rirang Sector (Figure) are strongly expected as a source of uranium and REE-bearing fluid. Uranium, REE, and several trace elements are commonly soluble in Na-rich rather than K-rich fluid. The occurrences of oligoclase and albite in the tourmaline and monazite ore characterize the Na-rich fluids. Moreover, Na-rich calc-silicate minerals such as hornblende associated with albite and oligoclase indicated the occurrence of sodic alteration [25]. On the other hand, the mineralization of brannerite, uranophane, and swamboite also indicated that the Na-metasomatism process occurred at medium temperatures [26]–[29]. The source of this metasomatism process is due to granitic intrusion in the north of the Rirang Sector and regionally correlated as Sukadana Granite.

The Rirang Sector is characterized by various mineralization and alteration processes that form several uranium and REE-bearing minerals, such as brannerite, uranophane, swamboite, monazite, xenotime, apatite, and loparite. Monazite, xenotime, apatite, and loparite are dominant LREE host minerals among these minerals. The high LREE/HREE ratio and negative Eu anomaly observed in the monazite ore indicated that these minerals originated from the felsic igneous source rocks.

In the samples studied, brannerite is the primary uranium-bearing mineral. This mineral cross-cuts the tourmaline and monazite ore, indicating that brannerite is formed in a later phase than both ores. Subsequently, brannerite is associated with pyrite, molybdenite, ilmenite, magnetite, rutile, and hematite, indicating the occurrence of the hydrothermal process during mineralization. Swamboite and uranophane are the later uranium mineral that formed resulting from the groundwater oxidation of brannerite [30].

The soil in the Rirang Sector, produced through weathering processes, exhibits a similar REE pattern to the host rocks and monazite ore. This similar pattern indicates an early phase leaching process of the monazite ore and host rock due to weathering [19], [20]. In some cases, weathering process can enrich the REE content in the soil [17], [28], [29], [31], with the main factor controlling the enrichment being clay minerals such as smectite, illite, kaolinite, and halloysite that act as adsorption agent of REE ions [19], [20], [32], [33]. In the Rirang sector, the clay mineral products are wonesite, illite, and kaolinite. Hence, the REE ions leach into the groundwater.

CONCLUSION

The Rirang Sector in West Kalimantan contains metapelite and metasiltstone that contain uranium and rare earth element (REE) mineralization. The dominant clay minerals in these rocks are derived from volcanic sources, and the alteration minerals are a product of hydrothermal alteration. Tourmaline and monazite ores are associated with uranium and REE mineralization. On the other hand, REE mineralization occurs in the form of monazite, xenotime, and loparite. The enrichment of uranium, REE, and other trace elements are believed to be due to their association with the Na-rich fluid of felsic intrusion. The north of the Rirang Sector's felsic intrusions correlates with the Sukadana Granite on the regional scale. The enrichment process of REE is apparently due to the fractional crystallization of felsic fluid

forming monazite, xenotime, apatite, and loparite. Furthermore, uranium enrichment is related to hydrothermal alteration, forming brannerite, uranophane, and other alteration minerals such as molybdenite, pyrite, copper, rutile, ilmenite, and magnetite. The interaction of the uranium-bearing mineral and groundwater forms secondary uranium mineral swamboite. The weathering process does not enrich the uranium and REE content in the soil but tend to decrease due to the leaching process and the absence of clay minerals that capable of binding REE ions into the soil.

ACKNOWLEDGMENT

The authors are grateful to the National Research and Innovation Agency for providing the funding and facility to conduct this investigation. We also thank the anonymous reviewers for their thorough reviews and helpful suggestions.

REFERENCES

[1] Ngadenin, A. Sumaryanto, H. Syaeful, and I. G. Sukadana, "Geologi dan Mineralisasi Uranium di Daerah Kalan, Kabupaten Melawi, Kalimantan Barat," in *Seminar Nasional Kebumian XII*, Yogyakarta: Fakultas Teknologi Mineral, Universitas Pembangunan Nasional "Veteran" Yogyakarta, 2017, pp. 108–114.

[2] Ngadenin, I. G. Sukadana, and R. Fauzi, "Preliminary overview of the prospects for rare earth elements in Kalan , West Kalimantan , Indonesia Preliminary Overview of The Prospects for Rare Indonesia," in *AIP Conference Proceedings*, 2022, pp. 1–11.

[3] Suharji, Ngadenin, Wagiyanto, and Sumarno, "Peningkatan Kwalitas Estimasi Cadangan Uranium dan Unsur Tanah Jarang Sebagai Asosiasinya di Sektor Rirang Hulu, Kalimantan Barat," *Pros. Semin. IPTEK Nukl. dan Pengelolaan Sumber Daya Tambang*, pp. 51–65, 2002.

[4] S. Tjokrokardono, "Studi Provinsi Uranium Kalimantan; Kajian Mineralisasi Uranium Pada Batuan Metamorf Dan Granit Di Pegunungan Schwaner," *Seminar IPTEK Nuklir dan Pengelolaan Sumber Daya Tambang*. 2002.

[5] S. Tjokrokardono, L. Subiantoro, and M. Widodo, "Sintesis Geologi dan Mineralisasi Uranium Kalan dan Sekitarnya, Kalimantan Barat," Jakarta, 2006.

[6] B. Soetopo, R. Witjahyati, and Y. Wusana, "Sintesa Geologi dan Pemineralan Uranium Sektor Rabau Hulu, Kalan, Kalimantan Barat," *Semin. Geol. Nukl. dan Sumberd. Tambang Tahun 2004*, pp. 85–99, 2004.

[7] D. Savira, M. A. Gunawan, W. A. Draniswari, I. G. Sukadana, and F. Sihombing, "μxRF Application for Uranium Exploration (Case Study: Mamuju Deposit, Indonesia)," *IOP Conf. Ser. Earth Environ. Sci.*, vol. 830, no. 1, 2021, doi: 10.1088/1755-1315/830/1/012076.

[8] I. G. Sukadana, I. W. Warmada, F. Pratiwi, A. Harijoko, T. B. Adimedha, and A. W. Yogatama, "Elemental Mapping for Characterizing of Thorium and Rare Earth Elements (REE) Bearing Minerals Using μXRF," *Atom Indones.*, vol. 48, no. 2, pp. 87–98, 2022, doi: 10.17146/aij.2022.1215.

[9] L. N. Warr, "IMA–CNMNC approved mineral symbols," *Mineral. Mag.*, vol. 85, no. 3, pp. 291–320, 2021, doi: 10.1180/mgm.2021.43.

[10] P. Alexandre, "Mineralogy and geochemistry of the sodium metasomatism-related uranium occurrence of Aricheng South, Guyana," *Miner. Depos.*, vol. 45, no. 4, pp. 351–367, 2010, doi: 10.1007/s00126-010-0278-7.

[11] J. A. Plant, P. R. Simpson, B. Smith, and B. F. Windley, "Uranium ore deposits-products of the radioactive earth," *Uranium Mineral. Geochemistry, Environ.*, no. September, pp. 255–319, 2019, doi: 10.1515/9781501509193-011.

[12] X. P. Yan, R. Kerrich, and M. J. Hendry, "Sequential leachates of multiple grain size fractions from a clay-rich till, Saskatchewan, Canada: Implications for controls on the rare earth element geochemistry of porewaters in an aquitard," *Chem. Geol.*, vol. 158, no. 1–2, pp. 53–79, 1999, doi: 10.1016/S0009-2541(99)00011-X.

[13] W. F. McDonough and S. s. Sun, "The composition of the Earth," *Chem. Geol.*, vol. 120, no. 3–4, pp. 223–253, 1995, doi: 10.1016/0009-2541(94)00140-4.

[14] S. M. McLennan, "Relationships between the trace element composition of sedimentary rocks and upper continental crust," *Geochemistry, Geophys. Geosystems*, vol. 2, 2001, doi: 10.1038/scientificamerican0983-130.

[15] S. R. Taylor and S. M. McLennan, *The continental crust: Its composition and evolution*. 1985.

[16] C. Wang, L. Zhang, Y. Dai, and C. Lan, "Geochronological and geochemical constraints on the origin of clastic meta-sedimentary rocks associated with the Yuanjiacun BIF from the Lüliang Complex, North China," *Lithos*, vol.

212–215, pp. 231–246, 2015, doi: 10.1016/j.lithos.2014.11.015.

[17] Z. Bao and Z. Zhao, "Rare-earth element mobility during ore-forming hydrothermal alteration: A case study of Dongping gold deposit, Hebei Province, China," *Chinese J. Geochemistry*, vol. 22, no. 1, pp. 45–57, 2003, doi: 10.1007/bf02831545.

[18] S. Akhtar, X. Yang, and F. Pirajno, "Sandstone type uranium deposits in the Ordos Basin, Northwest China: A case study and an overview," *J. Asian Earth Sci.*, vol. 146, no. September 2016, pp. 367–382, 2017, doi: 10.1016/j.jseaes.2017.05.028.

[19] Y. Kanazawa and M. Kamitani, "Rare earth minerals and resources in the world," in *Journal of Alloys and Compounds*, Feb. 2006, pp. 1339–1343. doi: 10.1016/j.jallcom.2005.04.033.

[20] A. Berger, E. Janots, E. Gnos, R. Frei, and F. Bernier, "Rare earth element mineralogy and geochemistry in a laterite profile from Madagascar," *Appl. Geochemistry*, vol. 41, pp. 218–228, 2014, doi: 10.1016/j.apgeochem.2013.12.013.

[21] G. W. A. Nyakairu and C. Koeberl, "Mineralogical and chemical composition and distribution of rare earth elements in clay-rich sediments from central Uganda," *Geochem. J.*, vol. 35, no. 1, pp. 13–28, 2001, doi: 10.2343/geochemj.35.13.

[22] B. K. Das, A. S. AL-Mikhlafi, and P. Kaur, "Geochemistry of Mansar Lake sediments, Jammu, India: Implication for source-area weathering, provenance, and tectonic setting," *J. Asian Earth Sci.*, vol. 26, no. 6, pp. 649–668, 2006, doi: 10.1016/j.jseaes.2005.01.005.

[23] R. Kritsananuwat, S. K. Sahoo, M. Fukushi, and S. Chanyotha, "Distribution of rare earth elements, thorium and uranium in Gulf of Thailand's sediments," *Environ. Earth Sci.*, vol. 73, no. 7, pp. 3361–3374, 2015, doi: 10.1007/s12665-014-3624-8.

[24] D. Bakkiaraj, R. Nagendra, R. Nagarajan, and J. S. Armstrong-Altrin, "Geochemistry of sandstones from the upper Cretaceous sillakkudi Formation, Cauvery basin, Southern India: Implication for provenance," *J. Geol. Soc. India*, vol. 76, no. 5, pp. 453–467, 2010, doi: 10.1007/s12594-010-0128-3.

[25] R. G. Skirrow *et al.*, *Uranium Mineral Systems : Processes , exploration criteria and a new deposit framework*. Geosciences Australia Record 2009/20, 2009.

[26] A. D. Mckay and Y. Miezitis, "Australia's uranium resources, geology and development of deposits.," 2001. doi: 10.1159/000335161.

[27] P. A. Polito and T. K. Kyser, "The Valhalla Uranium Deposit, Qeensland, Australia," *ASEG Ext. Abstr.*, vol. 2006, no. 1, pp. 1–4, 2006, doi: 10.1071/aseg2006ab140.

[28] M. Cuney and K. Kyser, "Recent and not-so-recent developments in uranium deposits and implications for exploration," *Short Course Ser. Vol. 39*, vol. 39, no. January 2009, p. 259, 2008.

[29] M. Cuney, A. Emetz, J. Mercadier, V. Mykchaylov, V. Shunko, and A. Yuslenko, "Uranium deposits associated with Na-metasomatism from central Ukraine: A review of some of the major deposits and genetic constraints," *Ore Geol. Rev.*, vol. 44, pp. 82–106, 2012, doi: 10.1016/j.oregeorev.2011.09.007.

[30] P. Bruneton and M. Cuney, *Geology of uranium deposits*, no. 1956. Elsevier Ltd, 2016. doi: 10.1016/B978-0-08-100307-7.00002-8.

[31] M. Bau, "Rare-earth element mobility during hydrothermal and metamorphic fluid-rock interaction and the significance of the oxidation state of europium," *Chem. Geol.*, vol. 93, no. 3–4, pp. 219–230, 1991, doi: 10.1016/0009-2541(91)90115-8.

[32] G. Estrade, E. Marquis, M. Smith, K. Goodenough, and P. Nason, "REE concentration processes in ion adsorption deposits: Evidence from the Ambohimirahavavy alkaline complex in Madagascar," *Ore Geol. Rev.*, vol. 112, no. March, p. 103027, 2019, doi: 10.1016/j.oregeorev.2019.103027.

[33] D. Wang *et al.*, "Exploration and research progress on ion-adsorption type REE deposit in South China," *China Geol.*, vol. 1, no. 3, pp. 414–423, 2018, doi: 10.31035/cg2018022.